LANGMUIR

pubs.acs.org/Langmuir Article

Unraveling How Cholesterol Affects Multivalency-Induced Membrane Deformation of Sub-100 nm Lipid Vesicles

Hyeonjin Park, Tun Naw Sut, Bo Kyeong Yoon, Vladimir P. Zhdanov, Nam-Joon Cho,* and Joshua A. Jackman*

Cite This: https://doi.org/10.1021/acs.langmuir.2c02252 Read Online

ACCESS | Metrics & More | Article Recommendations | Supporting Information

ABSTRACT: Cholesterol plays a critical role in modulating the lipid membrane properties of biological and biomimetic systems and recent attention has focused on its role in the functions of sub-100 nm lipid vesicles and lipid nanoparticles. These functions often rely on multivalent ligand−receptor interactions involving membrane attachment and dynamic shape transformations while the extent to which cholesterol can influence such interaction processes is largely unknown. To address this question, herein, we investigated the attachment of sub-100 nm lipid vesicles containing varying cholesterol fractions (0−45 mol %) to membrane-mimicking supported lipid bilayer (SLB) platforms. Biotinylated lipids and streptavidin proteins were used as model ligands and receptors, respectively, while the localized surface plasmon resonance sensing technique was employed to track vesicle attachment kinetics in combination with analytical modeling of vesicle shape changes. Across various conditions mimicking low and high multivalency, our findings revealed that cholesterol-containing vesicles could bind to receptor-functionalized membranes but underwent appreciably less multivalency-induced shape deformation than vesicles without cholesterol, which can be explained by a cholesterol-mediated increase in membrane bending rigidity. Interestingly, the extent of vesicle deformation that occurred in response to increasingly strong multivalent interactions was less pronounced for vesicles with greater cholesterol fraction. The latter trend was rationalized by taking into account the strong dependence of the membrane bending energy on the area of the vesicle−SLB contact region and such insights can aid the engineering of membrane-enveloped nanoparticles with tailored biophysical properties.

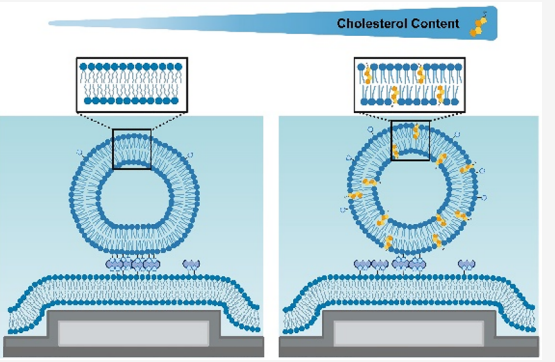

INTRODUCTION

Cholesterol is a naturally occurring sterol that is found in biological membranes and plays an important role in modulating membrane properties such as fluidity, permeability, and rigidity.[1,2] Structurally, the molecular-level interactions of cholesterol and phospholipids affect membrane packing and the phase state, which influences dynamic biological processes such as membrane fusion and endocytosis.[3] Within this context, increasing attention has been placed on understanding how cholesterol affects the biophysical properties of biomimetic lipid vesicle and lipid nanoparticle (LNP) delivery vehicles that are used for vaccine and therapeutic applications.[4,5] Such efforts have heightened interest in studying the effects of cholesterol on membrane nanomechanical properties[6,7] in order to rationally design LNPs with tailored properties.[8,9]

In general, membrane nanomechanical properties depend on the membrane composition and phase state. Within this context, it is noteworthy that cholesterol tends to induce the formation of nano- and microdomains in lipid membranes.[1,2] Usually, this effect is observed in bi- or multicomponent membranes containing saturated and unsaturated lipids and associated with preferential interactions between cholesterol and saturated lipids.[1] Cholesterol-rich regions have been found around transmembrane proteins as well.[1] Concerning membrane nanomechanical properties, one can find numerous studies scrutinizing the effect of cholesterol fraction on lipid membrane mechanics with respect to membrane composition and curvature [e.g., by utilizing high-curvature, small unilamellar vesicles (SUVs) and low-curvature, giant unilamellar vesicles (GUVs) of around <300 nm and >5 μm diameters, respectively, along with planar supported lipid bilayers (SLBs)], and the main focus has been measuring the membrane bending modulus, which describes the mechanical strength of a lipid bilayer to resist deformation.[10−12] Accordingly, a larger bending modulus indicates greater

Received: August 19, 2022
Revised: October 30, 2022

mechanical strength and more resistance to deformation in response to an applied strain.

Several studies have reported that the bending modulus of a lipid bilayer increases in the presence of cholesterol when the bilayer is composed of phospholipids with saturated hydrocarbon chains.[13,14] However, the effect of cholesterol on the bending modulus of lipid bilayers composed of unsaturated phospholipids, especially 1,2-dioleoyl-*sn*-glycero-3-phosphocholine (DOPC) lipids, is more widely debated. A few studies have reported that cholesterol inclusion causes densification-related stiffening of DOPC lipid bilayers and, hence, an increased bending modulus, as demonstrated in experimental models based on GUVs[15,16] and SUVs,[17] as well as in computational simulations.[6] Conversely, other studies have determined that cholesterol inclusion causes no change in the bending modulus of lipid bilayers using GUV[18] and SUV[19] models while also noting that cholesterol can induce membrane densification and a corresponding decrease in water permeability.[20] Regarding these details, it deserves attention that cholesterol molecules can easily undergo flip-flop and, thus, relax local stresses induced by bending deformations.[21]

Unraveling how cholesterol affects the nanomechanical properties of DOPC lipid bilayers in more biologically significant contexts would complement the aforementioned studies, especially as molecular components such as DOPC are increasingly used as helper lipids in LNP delivery vehicles.[22,23] Toward this goal, the atomic force microscopy (AFM) technique has been useful for investigating how a larger cholesterol fraction can increase the bending modulus of sub-100 nm lipid vesicles, which have high membrane curvature[24] and are within the typical size range used for biomedical applications. Such efforts fit within a broader set of AFM-based experimental efforts[25,26] to deposit nonspecifically adsorbed biomimetic and cell-derived lipid vesicles onto glass surfaces and to study how adsorbed vesicles deform in response to mechanical strain induced by the AFM cantilever tip. As sub-100 nm lipid vesicles are models of membrane-enveloped exosomes and virus particles that exhibit biological functions related to receptor-mediated cell membrane interactions and corresponding shape deformation processes, it would be opportune to expand on these biophysical approaches to utilize cell-membrane-mimicking platforms that involve receptor-mediated binding in a more selective manner. Indeed, multivalent ligand−receptor interactions at cell membrane interfaces are central to the biological functions of ligand-modified exosomes, virus particles, lipid vesicles, and LNPs and hence rationalizing how such interactions are affected by the presence of cholesterol in lipid membranes is an outstanding need.

Herein, using a receptor-modified SLB platform, we investigated how cholesterol fraction in ligand-modified DOPC lipid vesicles affects multivalent ligand−receptor interactions in terms of vesicle attachment kinetics onto the SLB platform and corresponding shape changes in attached vesicles. Central to our experimental approach was the label-free localized surface plasmon resonance (LSPR) technique, in which a receptor-functionalized SLB platform was conformally coated on a silica-coated sensor chip and the specific attachment of ligand-modified lipid vesicles to the SLB platform was tracked in real-time by measuring changes in the local refractive index near the sensor surface.[27−29] Using an analytical model to quantify the LSPR measurement signals, we identified how the cholesterol fraction in lipid vesicles affects multivalency-engaged vesicle attachment and the subsequent shape deformation of attached vesicles by further stiffening lipid membranes even in the high membrane-curvature regime.

MATERIALS AND METHODS

Materials. 1,2-Dioleoyl-*sn*-glycero-3-phosphocholine (DOPC), 1,2-dihexanoyl-*sn*-glycero-3- phosphocholine (DHPC), and 1,2-dioleoyl-*sn*-glycero-3-phosphoethanolamine-*N*-(cap biotinyl) (DOPE-Biotin) lipids in chloroform were obtained from Avanti Polar Lipids (Alabaster, AL). Cholesterol in dry powder form (ovine wool, >98%) was obtained from Avanti Polar Lipids (Alabaster, AL). Streptavidin in lyophilized form (catalog no. S203) was purchased from Leinco (St. Louis, MO). Free biotin in lyophilized form (catalog no. B4639) and other reagents were obtained from Sigma-Aldrich (St. Louis, MO). Aqueous buffer solution [10 mM Tris (pH 7.5) and 150 mM NaCl] was prepared using Milli-Q-treated water (>18 MΩ·cm; MilliporeSigma, Burlington, MA).

Sample Preparation. Lipid bicelles composed of long-chain phospholipids (DOPC and DOPE-Biotin) and short-chain phospholipid (DHPC) with a molar ratio of [DOPC + DOPE-Biotin] to [DHPC] of 0.25 and total lipid concentration of 5 mM were prepared by freeze−thaw−vortex processing in order to fabricate biotinylated SLBs on silica-coated sensor surfaces, as previously described.[30] During SLB formation, long-chain lipids self-assemble into a planar SLB while short-chain lipids do not reside within the SLB and are washed away into the bulk solution, eventually being removed upon buffer washing. Vesicles consisting of DOPC, DOPE-Biotin, and cholesterol were prepared by the extrusion method.[31] Briefly, cholesterol powder was dissolved in chloroform and mixed with DOPC and DOPE-Biotin phospholipids at a lipid concentration of 5 mg/mL, followed by drying, hydration, and extrusion through track-etched polycarbonate membranes with 50 nm pore diameter. The exact molar compositions of the three lipids in each vesicle sample are described in Table S1, while the mol % DOPC listed below more precisely refers to mol % of [DOPC + DOPE-Biotin] (since the two long-chain phospholipids were mixed), and the biotinylated lipid fraction (i.e., mol % DOPE-Biotin) is described explicitly for clarity when describing experimental results. The vesicle populations had around 70 ± 2, 75 ± 2, 79 ± 2, and 82 ± 3 nm mean diameters for vesicles with 0, 15, 30, and 45 mol % cholesterol fractions, respectively, as determined by dynamic light scattering (DLS) measurements. Immediately before the experiment, the bicelle and vesicle samples were diluted ∼32- and 50-times in Tris buffer solution, respectively. Streptavidin protein was dissolved in Milli-Q-treated water at a concentration of 24 μM and then diluted in Tris buffer by ∼24-times before the experiment. A 2 mM free biotin stock solution was prepared in Tris buffer and diluted in Tris buffer by ∼1000-fold before the experiment.

Localized Surface Plasmon Resonance (LSPR) Sensing. LSPR measurements were performed on silica-coated silver nanodisk arrays by using an Insplorion XNano instrument (Insplorion AB, Gothenburg, Sweden), which is based on an indirect nanoplasmonic sensing concept. The sensing platform consisted of silver nanodisk transducers (∼100 nm diameter and ∼20 nm height) on a glass substrate and the entire sensing surface was conformally covered with an ∼10 nm thick layer of silicon nitride.[32,33] The silver nanodisk arrays were fabricated by hole-mask colloidal lithography and had ∼8% of surface coverage.[34] Prior to experiment, the sensor chips were rinsed with ethanol and dried with nitrogen gas, followed by treatment with oxygen plasma for 1 min by using a CUTE-1MPR machine (Femto Science Inc., Hwaseong, Republic of Korea). The latter step led to the formation of a silica overlayer on the silicon nitride surface.[35] Afterward, the silica-coated sensor chip was loaded into a microfluidic chamber and liquid samples were injected under continuous flow conditions at a flow rate of 50 μL/min using a peristaltic pump (Reglo Digital MS-4/6, Ismatec, Glattsburg, Switzerland). Of note, the cross-section and length of the flow channel are around 1 × 2 and 5 mm, respectively, and hence the

https://doi.org/10.1021/acs.langmuir.2c02252
Langmuir XXXX, XXX, XXX−XXX

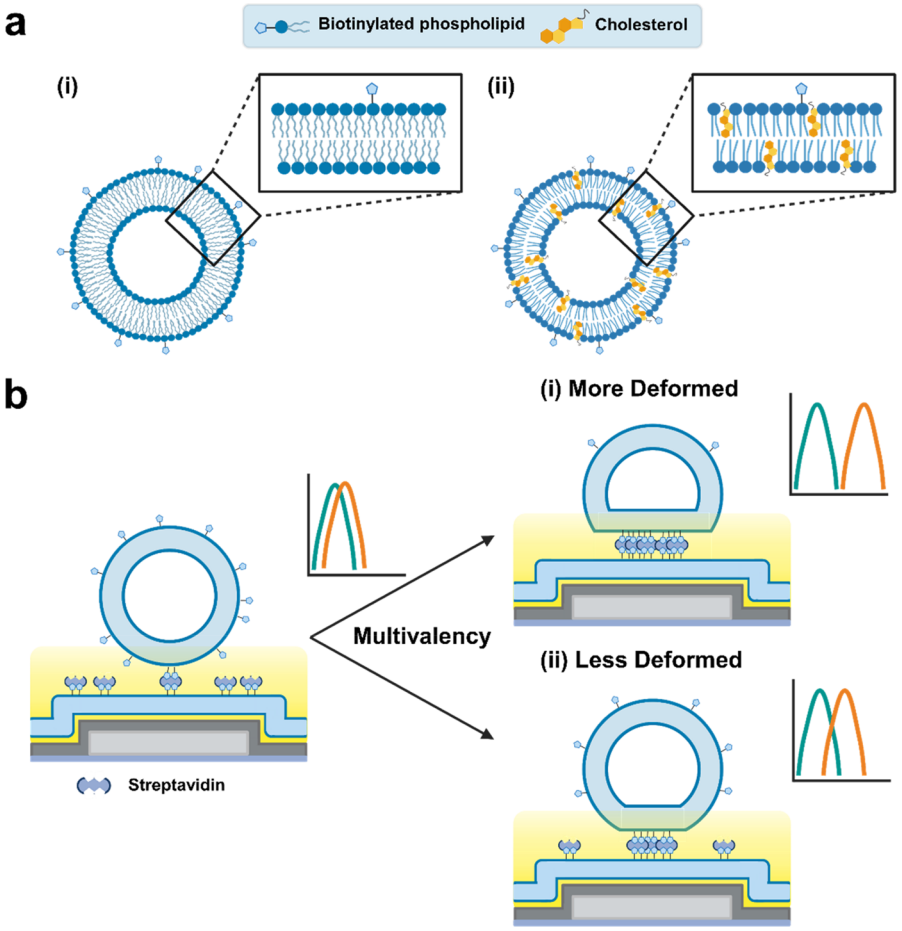

Figure 1. Experimental strategy to investigate how cholesterol affects multivalency-induced shape deformation of sub-100 nm lipid vesicles. (a) Schematic illustration of biotinylated DOPC lipid vesicles containing (i) no cholesterol or (ii) variable fractions of cholesterol (15, 30, or 45 mol %). Note that cholesterol incorporation can influence membrane packing. (b) Overview of LSPR measurement approach to characterize deformation of vesicles (without or with cholesterol) during their attachment to the SLB (without cholesterol). When there is greater deformation, the lipid mass will be, on average, in a region of higher LSPR-enhanced field intensity near the sensor surface, which results in a larger measurement response. This is figuratively shown by drawing one vesicle at the center of an LSPR nanodisk. In reality, vesicles are attached in a more or less random manner like in the random sequential adsorption model.[37] This arrangement of attached vesicles is also implied in our analysis of the related LSPR signal.

average flow velocity, v_0, was calculated to be 25 mm/min.[32] During experiments, the optical extinction spectrum of transmitted white light passing through the sensor chip was measured by UV−vis spectroscopy and collected with a time resolution of 1 Hz. The LSPR peak wavelength that corresponds to the maximum-intensity extinction wavelength (denoted as λ_{max}) in each spectrum was determined by the centroid method,[36] and data analyses were conducted using the Insplorer software package (Insplorion AB).

RESULTS AND DISCUSSION

Measurement Strategy. Figure 1a presents a schematic illustration of sub-100 nm lipid vesicles that (i) contain DOPC phospholipids only and no cholesterol or (ii) a mixture of DOPC phospholipids and cholesterol. Typically, fluid-phase DOPC lipid bilayers are relatively flexible while cholesterol incorporation can affect the membrane phase properties, giving rise to liquid-disordered or liquid-ordered phase states depending on the overall membrane composition and cholesterol fraction. It should be emphasized that such findings have been mainly obtained from planar and low-curvature model membranes while, for sub-100 nm lipid vesicles, the membrane is in the high-curvature regime where curvature-induced membrane stiffening can be appreciable by itself and the corresponding membrane bending energy of a sub-100 nm lipid vesicles can be quite large. In the latter high membrane-curvature regime, the effect of cholesterol incorporation on membrane nanomechanical properties is less understood because the contribution of cholesterol-induced membrane stiffening must be considered within the broader context of curvature-induced stiffening effects.

To address this gap, we utilized the LSPR technique in order to track the real-time adsorption of biotinylated vesicles onto a streptavidin-coated SLB platform (Figure 1b). The biotin−streptavidin interaction is one of the strongest noncovalent interactions in nature and is a widely used model system to study multivalent ligand−receptor binding in general. In our system, the lipid vesicles contained a tunable amount of biotinylated lipids (ligands) while there was a fixed amount of streptavidin proteins (receptors) on the SLB platform interface. Depending on the balance between the membrane bending energy and the multivalent ligand−receptor interaction energy, attached lipid vesicles will undergo more or less shape deformation, which can be detected by the LSPR measurement readout.

https://doi.org/10.1021/acs.langmuir.2c02252
Langmuir XXXX, XXX, XXX−XXX

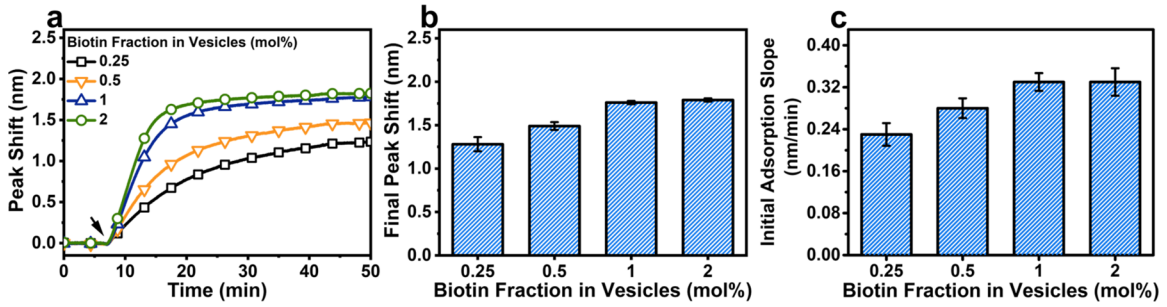

Figure 2. LSPR tracking of 100 mol % DOPC lipid vesicle attachment to streptavidin-coated supported lipid bilayer. (a) Time-resolved $\Delta\lambda_{max}$ shifts for vesicle addition to streptavidin-coated SLB platform. The molar fraction of biotinylated lipids in the vesicles was adjusted from 0.25 to 2 mol %. Vesicle addition started from t = 7 min and a buffer washing step was conducted from t = 47 min onward. (b) Final $\Delta\lambda_{max}$ shifts corresponding to vesicle attachment at saturation and (c) rate of change in the $\Delta\lambda_{max}$ signal during the initial attachment stage [in panel (a)]. Data in panels (b) and (c) are represented as mean ± standard deviation from three independent experiments.

The SLB platform was fabricated on a silica-coated nanoplasmonic sensor chip and UV−visible spectroscopy experiments were performed in transmission mode to track SLB fabrication and subsequent vesicle attachment, including shape deformation. The interaction of white light with the plasmonic nanodisks induces the coherent oscillation of conduction-band electrons near the nanodisk surface, which arises from the LSPR optical phenomenon and is characterized by a maximum-intensity emission wavelength (λ_{max}) in the corresponding optical extinction spectrum. In this case, the electromagnetic field is enhanced near the sensor surface (~5−10 nm decay length), allowing one to sensitively detect changes in the local refractive index that can be measured by a $\Delta\lambda_{max}$ shift. For example, lipid molecules have a greater refractive index than water molecules so an adsorbed lipid vesicle will increase the local refractive index relative to an aqueous buffer baseline, which can be detected by a positive $\Delta\lambda_{max}$ shift (Figure S1). Importantly, the time-resolved $\Delta\lambda_{max}$ shift is sensitive to both the number and shape of attached vesicles and analytical modeling can extract quantitative information about vesicle shape deformation in the low and high surface coverage regimes. In general, greater deformation of an attached vesicle results in the lipid mass being, on average, in a region of higher field intensity closer to the sensor surface that translates into a larger $\Delta\lambda_{max}$ shift.

In our experiments, a flow-through microfluidic chamber was used to house the silica-coated silver nanodisk array and we fabricated conformal SLBs on top of the sensor surface by using lipid bicelles containing 99 mol % DOPC lipid and 1 mol % DOPE-Biotin lipid (Figure S2). Afterward, streptavidin molecules were added and became firmly attached to available biotinylated lipid ligands on the SLB platform, yielding a streptavidin-coated SLB platform whereby streptavidin proteins acted as model receptors to mediate specific binding interactions with biotinylated lipid vesicles. Since the molar fraction of biotinylated lipids in the SLB platform was consistent, the number of attached streptavidin molecules and hence the corresponding receptor density in the SLB were fixed in the experiments (Figure S3).

Then, ~75 nm diameter DOPC lipid vesicles containing 0, 15, 30, or 45 mol % cholesterol were injected into the microfluidic chamber under continuous flow conditions and gradually became attached to the streptavidin-coated SLB platform. The corresponding vesicle attachment process was tracked by monitoring the time-resolved $\Delta\lambda_{max}$ shift relative to the baseline signal prior to vesicle addition. To facilitate vesicle attachment, the lipid vesicles also contained 0.25, 0.5, 1, or 2 mol % biotinylated lipid (DOPE-Biotin), which enabled specific binding to the streptavidin-coated SLB and a larger fraction of biotinylated lipids contributed to a stronger multivalent ligand−receptor binding interaction energy. This compositional tuning allowed us to elucidate how cholesterol fraction influences vesicle attachment and resulting shape deformation processes across the tested range of experimental scenarios ranging from relatively low to high multivalency conditions. In Figures 2−5 below, the LSPR measurement baselines refer to the streptavidin-coated SLB platform and the presented time-resolved $\Delta\lambda_{max}$ shifts depict the vesicle attachment step whereby both the final $\Delta\lambda_{max}$ shift at saturation and the initial rate of change in the $\Delta\lambda_{max}$ signal in the low-coverage regime were scrutinized.

LSPR Measurements. Figure 2a shows time-resolved $\Delta\lambda_{max}$ shifts for 100 mol % DOPC lipid vesicles with a biotinylated lipid fraction of 0.25 to 2 mol % during their attachment to the streptavidin-coated SLB. Monotonic adsorption occurred until there was saturation of attached vesicles for all samples and the resulting final $\Delta\lambda_{max}$ shifts for vesicle attachment were larger when vesicles had a greater biotin ligand density. For 0.25 and 0.5 mol % biotinylated lipid vesicles, the final $\Delta\lambda_{max}$ shifts were 1.28 ± 0.08 and 1.49 ± 0.04 nm, respectively (Figure 2b). The final $\Delta\lambda_{max}$ shift further increased to 1.76 ± 0.02 nm for 1 mol % biotinylated lipid vesicles while a similar $\Delta\lambda_{max}$ shift of 1.79 ± 0.02 nm was observed for vesicles with 2 mol % biotinylated lipid fraction. The final $\Delta\lambda_{max}$ shift magnitude depends on both the surface concentration and deformation of attached vesicles,[32] which led us to further investigate vesicle deformation in the low surface-coverage regime.

Specifically, we analyzed the rate of change in the $\Delta\lambda_{max}$ signal during the initial vesicle attachment stage, which reflects the relative degree of multivalency-induced vesicle shape deformation (Figure 2c).[38,39] In general, a larger rate implies greater shape deformation of attached vesicles on a comparative basis. The rate was around 0.23 ± 0.02 nm/min for 0.25 mol % biotinylated lipid vesicles and further increased to around 0.28 ± 0.02, 0.33 ± 0.02, and 0.33 ± 0.03 nm/min for the 0.5, 1, and 2 mol % biotinylated lipid vesicle cases, respectively. Hence, a greater degree of multivalent biotin−streptavidin binding interactions triggered the attached vesicles to deform to a greater extent until a critical density of such interactions was reached, which agrees well with our past

https://doi.org/10.1021/acs.langmuir.2c02252
Langmuir XXXX, XXX, XXX−XXX

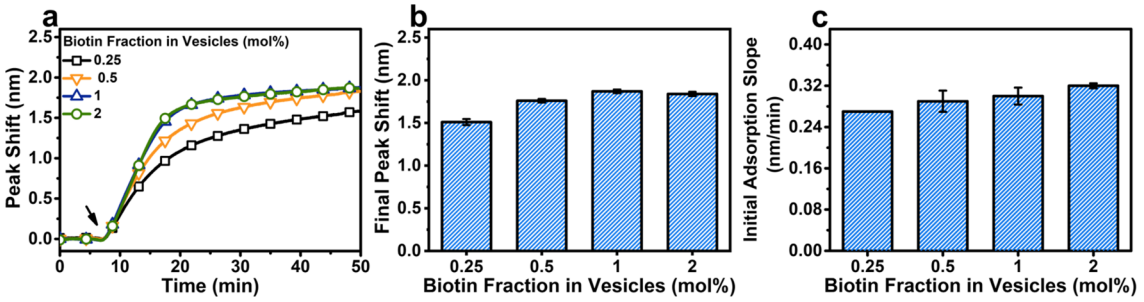

Figure 3. LSPR tracking of 85/15 mol % DOPC/cholesterol vesicle attachment to streptavidin-coated supported lipid bilayer. (a) Time-resolved $\Delta\lambda_{max}$ shifts for vesicle addition to streptavidin-coated SLB platform. (b) Final $\Delta\lambda_{max}$ shifts corresponding to vesicle attachment at saturation and (c) rate of change in the $\Delta\lambda_{max}$ signal during the initial attachment stage [in panel (a)]. The panels are depicted as in Figure 2.

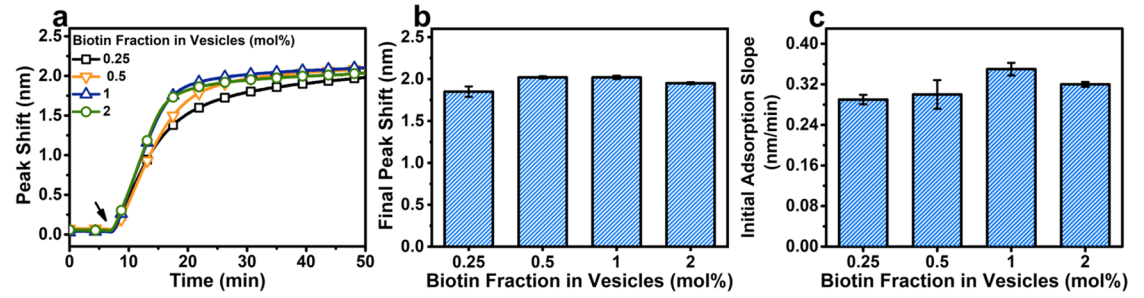

Figure 4. LSPR tracking of 70/30 mol % DOPC/cholesterol vesicle attachment to streptavidin-coated supported lipid bilayer. (a) Time-resolved $\Delta\lambda_{max}$ shifts for vesicle addition to streptavidin-coated SLB platform. (b) Final $\Delta\lambda_{max}$ shifts corresponding to vesicle attachment at saturation and (c) rate of change in the $\Delta\lambda_{max}$ signal during the initial attachment stage [in panel (a)]. The panels are depicted as in Figure 2.

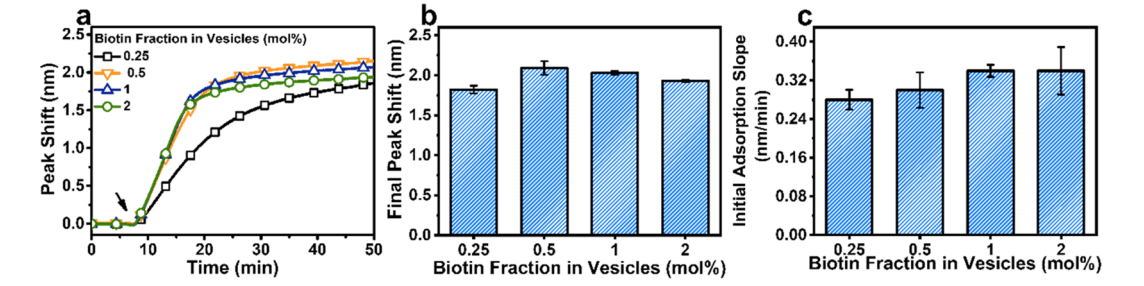

Figure 5. LSPR tracking of 55/45 mol % DOPC/cholesterol vesicle attachment to streptavidin-coated supported lipid bilayer. (a) Time-resolved $\Delta\lambda_{max}$ shifts for vesicle addition to streptavidin-coated SLB platform. (b) Final $\Delta\lambda_{max}$ shifts corresponding to vesicle attachment at saturation and (c) rate of change in the $\Delta\lambda_{max}$ signal during the initial attachment stage [in panel (a)]. The panels are depicted as in Figure 2.

findings[27] and provides a quantitative basis to evaluate the effects of cholesterol incorporation in the vesicles.

We proceeded to track the time-resolved $\Delta\lambda_{max}$ shifts for 85/15 mol % DOPC/cholesterol vesicle attachment to the streptavidin-coated SLB platform (Figure 3a). Again, vesicle attachment reached a saturation point for all samples, and the final $\Delta\lambda_{max}$ shifts were generally larger than in the case of 100 mol % DOPC lipid vesicles, which reflects the higher refractive index of the DOPC/cholesterol lipid bilayer as compared to that of a DOPC lipid bilayer.[40] For 0.25 and 0.5 mol % biotinylated lipid vesicles, the final $\Delta\lambda_{max}$ shifts at saturation were around 1.51 ± 0.04 and 1.76 ± 0.02 nm, respectively (Figure 3b). The final $\Delta\lambda_{max}$ shifts further increased to similar values of around 1.87 ± 0.02 and 1.84 ± 0.02 nm for 1 and 2 mol % biotinylated lipid vesicles, respectively. It should be noted that, as the molar fraction of biotinylated lipids in the vesicles increased, the relative magnitude of the $\Delta\lambda_{max}$ shift values increased by only 24% for the 85/15 mol % DOPC/cholesterol vesicles, whereas the corresponding increase was 40% in the case of 100 mol % DOPC lipid vesicles described above.

In addition, the rate of change in the $\Delta\lambda_{max}$ signal during the initial vesicle attachment stage was around 0.27 nm/min for 85/15 mol % DOPC/cholesterol vesicles with 0.25 mol % biotinylated lipid fraction, and increased to around 0.29 ± 0.02, 0.30 ± 0.02, and 0.32 ± 0.01 nm/min for the 0.5, 1, and 2 mol % biotinylated lipid vesicle cases, respectively (Figure 3c). In this case, the relative magnitude of the rate increased by only 19% as the molar fraction of biotinylated lipids in the vesicles increased from 0.25 to 2 mol %, which was appreciably smaller than the 43% increase for 100 mol % DOPC lipid vesicles across the same range. These quantitative trends support that the extent of deformation of cholesterol-enriched vesicles is also affected by multivalent ligand−receptor interactions while the magnitude of such effects is smaller than for fluid-phase lipid vesicles lacking cholesterol and indicates a deformation-suppressing effect of cholesterol.

These findings led us to further increase the cholesterol fraction in the vesicles to 30 mol % and the corresponding

https://doi.org/10.1021/acs.langmuir.2c02252
Langmuir XXXX, XXX, XXX−XXX

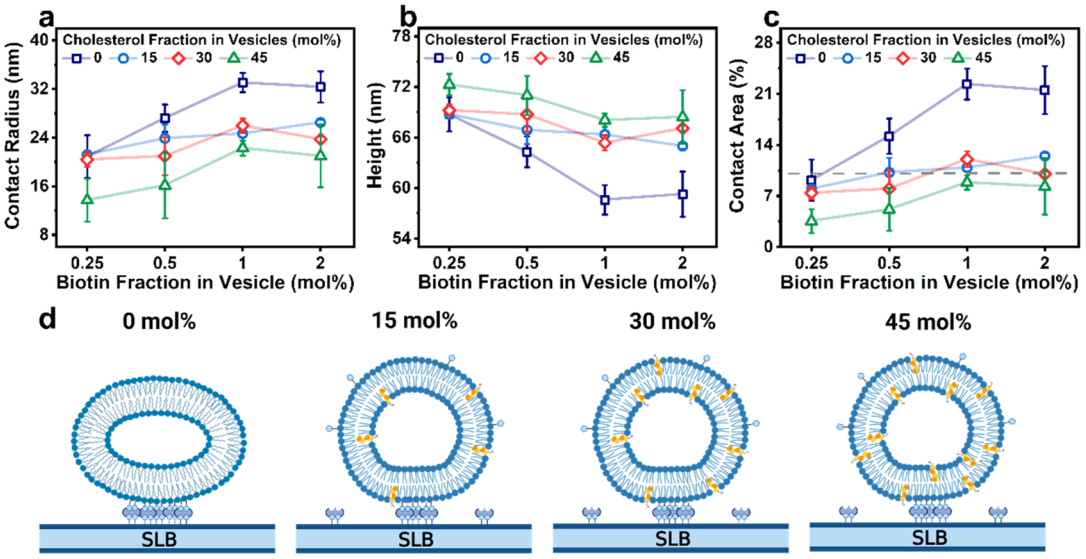

Figure 6. Biophysical characterization of multivalency-induced shape deformation for cholesterol-enriched vesicles. (a) Contact radius and (b) height of adsorbed vesicles as a function of molar fraction of biotinylated lipids in the vesicles. The analytical modeling was performed for vesicles with different cholesterol fractions based on the data in Figures 2−5. (c) Corresponding percentage of the vesicle surface area contacting SLB relative to the total vesicle surface area as a function of the molar fraction of biotinylated lipids in the vesicles. Dashed line indicates the 10% mark [vesicle deformation is often described as appreciable when the percentage is higher than 10% (see ref 27 and references therein)]. (d) Schematic illustration describing how cholesterol fraction affects the multivalency-induced structural deformation of attached vesicles.

time-resolved $\Delta\lambda_{max}$ shifts for vesicle attachment to the streptavidin-coated SLB platform are presented in Figure 4a. In this case again, similar monotonic adsorption behavior was observed while the final $\Delta\lambda_{max}$ shifts at saturation were typically larger, which also reflects a larger refractive index of the lipid bilayer at higher cholesterol fractions as mentioned above. The final $\Delta\lambda_{max}$ shifts were around 1.85 ± 0.06 and 2.02 ± 0.01 nm for 70/30 mol % DOPC/cholesterol vesicles with 0.25 and 0.5 mol % biotinylated lipid fractions, respectively (Figure 4b). Similar final $\Delta\lambda_{max}$ shifts of around 2.02 ± 0.02 and 1.95 ± 0.01 nm were also observed for the 1 and 2 mol % biotinylated lipid vesicle cases, respectively. In addition, the rates of change in the $\Delta\lambda_{max}$ signal hovered around ∼0.32 nm/min for vesicles across all tested biotinylated lipid fractions and there was no dependence of the rate on the cholesterol fraction in the vesicles (Figure 4c).

We also investigated vesicle attachment to the streptavidin-coated SLB platform for 55/45 mol % DOPC/cholesterol vesicles and the time-resolved $\Delta\lambda_{max}$ shifts indicated monotonic adsorption behavior for vesicles across all tested biotinylated lipid fractions (Figure 5a). The final $\Delta\lambda_{max}$ shift was around 1.82 ± 0.05 nm for 0.25 mol % biotinylated lipid vesicles and further increased to around 2.09 ± 0.09, 2.03 ± 0.02, and 1.93 ± 0.01 nm for 0.5, 1, and 2 mol % biotinylated lipid vesicles, respectively (Figure 5b). A similar trend in the initial rates of change in the $\Delta\lambda_{max}$ signal was also observed, whereby the rate was 0.28 ± 0.02 nm/min for 0.25 mol % biotinylated lipid vesicles and increased to around 0.30 ± 0.04, 0.34 ± 0.01, and 0.34 ± 0.05 nm/min for 0.5, 1, and 2 mol % biotinylated lipid vesicles, respectively (Figure 5c). Hence, the overall trends were similar to the 70/30 mol % DOPC/cholesterol vesicle case and indicated that greater multivalency at higher biotinylated lipid fractions had less effect on the LSPR measurement responses than in the cases of lipid vesicles with appreciably less or no cholesterol.

We further analyzed the LSPR measurement data to extract quantitative details about multivalency-induced deformation of attached vesicles and the corresponding effect of cholesterol incorporation in the lipid vesicles (sections 4 and 2 in the Supporting Information and refs 27 and 28, respectively). In our analytical model, a deformed vesicle was treated as a truncated sphere with radius R_v and basement radius r, and we obtained quantitative estimates of r, the deformation-related height of an attached vesicle (h), and the surface area of the vesicle-SLB contact region (πr^2), from the experimentally measured rates of change in the $\Delta\lambda_{max}$ signal during the initial vesicle attachment stage (section 1 in the Supporting Information and Table S2).

Vesicle Deformation Analysis. Figure 6a−c show the contact radius and height, r and h, of an attached vesicle as well as the fractional percentage of the total vesicle surface area, $4\pi R^2$, that contacts the SLB interface, πr^2. From these plots, three general trends can be observed:

First, higher biotinylated lipid fractions lead to an increase in the contact radius magnitude and decrease in the vesicle height because they enable a greater possible number of biotin−streptavidin complexes to be formed in the vesicle-SLB contact region and hence a stronger multivalent binding energy that opposed the membrane bending energy. For 100 mol % DOPC lipid vesicles, the contact radius increased from ∼21 to ∼32 nm as the molar fraction of biotinylated lipids in the vesicles changed from 0.25 to 2 mol %, which corresponds to a 52% increase in the contact radius value as the degree of multivalency increased in the system. The corresponding contact radii of attached vesicles increased from ∼21 to ∼26 nm and from ∼20 to ∼24 nm for 85/15 and 70/30 mol % DOPC/cholesterol vesicles, respectively, which reflect 24% and 20% increases in the contact radius values for these two cases. For 55/45 mol % DOPC/cholesterol vesicles, the corresponding contact radius increased from ∼14 to ∼21 nm, which translates into a 50% increase but still relatively low value.

Second, a higher cholesterol fraction in vesicles led to a decrease in the contact radius magnitude and an increase in

https://doi.org/10.1021/acs.langmuir.2c02252
Langmuir XXXX, XXX, XXX−XXX

vesicle height. This feature can be explained mainly by a cholesterol-mediated increase in the lipid bilayer bending rigidity and partly by a decrease in the amount of biotinylated lipid with increasing cholesterol fraction (this is the case because the size of the interface area of the fabricated vesicles is kept constantly independent of the cholesterol fraction, and accordingly, increasing the cholesterol fraction decreases the amount of phospholipid in general and biotinylated phospholipid in particular).

Third, an increase in the contact radius magnitude and a decrease in the vesicle height, observed with increasing biotinylated lipid fraction, become less manifested for vesicles with increasing cholesterol fraction. In particular, these effects are nearly negligible for the 55/45 mol % DOPC/cholesterol lipid vesicles. This feature reflects a similar dependence of the results shown in Figures 3−5.

At first sight, the third general trend might be unexpected. To rationalize this trend, we recall our earlier interpretation[27] of the results obtained without cholesterol (cf. Figures 2 and 6) where the dependence on the biotinylated lipid fraction is appreciable for the 0.25, 0.5, and 1 mol % cases and nearly negligible when increasing this fraction from 1 to 2 mol %. In general, as already noticed, this dependence depends on the interplay of the membrane bending energy and the multivalent ligand−receptor interaction energy. In our case, the ligand−receptor interaction is fairly strong and induces translocation of biotinylated lipids to the vesicle-SLB contact region. If the biotinylated lipid fraction, f_{b1}, is small, then the contact region is rather small even though all of the biotinylated lipids are there, and this is possible because the corresponding changes in the membrane bending energy are small (smaller than the gain in energy due to the formation of ligand−receptor pairs). In this case, the area of the contact region can be estimated as $\pi r^2 \simeq n_{b1}s = f_{b1}n_l s$, where n_{b1} is the number of biotinylated lipids in the outer leaflet of a vesicle, n_l is the total number of lipids in this leaflet of a vesicle, and s is the area corresponding to one ligand−receptor pair. With increasing biotinylated lipid fraction, the bending energy rapidly increases and the translocation of all the biotinylated lipids to face the contact region becomes energetically unfavorable. Hence, the dependence of the contact area (or radius) on biotinylated lipid fraction becomes weaker, in some cases appreciably so. In the absence of cholesterol, this occurs when increasing the biotinylated lipid fraction from 1 to 2 mol %. With cholesterol, the bending rigidity becomes higher, and it appears to happen already when the biotinylated lipid fraction is low, ≃0.25−0.5 mol %. These arguments explain the third general trend and also why the contact radius (or area) decreases with increasing cholesterol fraction even when the biotinylated lipid fraction is low.

Figure 6d presents a schematic summary of our experimental observations discussed above.

In addition to analyzing how the initial rates of change in the $\Delta\lambda_{max}$ signal relate to multivalency-induced vesicle shape deformation, we also applied this modeling approach to determine the surface concentration of attached vesicles from the final $\Delta\lambda_{max}$ shifts at saturation (cf. Figures 2−5). The surface concentration of attached vesicles was around 70−80 vesicles per μm^2 and did not depend on the cholesterol fraction or biotinylated lipid fraction in the vesicles (Table S3). This finding is consistent with our past report[27] that demonstrated changing the biotinylated lipid fraction in the SLB itself, but not in the vesicles, affects vesicle surface coverage, while the biotinylated lipid fraction in the SLB was fixed at 1 mol % in the present experiments. These surface concentration calculations further reinforce that, for each lipid composition, larger $\Delta\lambda_{max}$ shifts at saturation mainly reflect a greater degree of vesicle deformation, which agrees well with our analysis of the rate of change in the $\Delta\lambda_{max}$ signal in the low surface coverage regime as described above.

Returning to the question of how cholesterol affects the nanomechanical properties of DOPC lipid bilayers, our findings indicate that cholesterol incorporation into sub-100 nm DOPC lipid vesicles increases membrane bending energy, which was supported by our observation that there was less multivalency-induced vesicle shape deformation compared to vesicles without cholesterol. While previous studies have discussed how cholesterol stiffens lipid membranes in general,[17,41] the nanomechanical properties of sub-100 nm lipid vesicles are typically measured by AFM-based tip indentation in a perturbative manner and when the vesicles are adsorbed nonspecifically to a surface. In marked contrast, our experimental platform investigated how sub-100 lipid vesicles containing cholesterol undergo shape deformation in a label-free, nonperturbative manner due to biologically relevant multivalent interactions that involve specific binding to membrane-associated receptors. Obtaining information about the membrane bending properties of high-curvature membranes in this size regime is challenging and current knowledge supports that the membrane bending energy of sub-100 nm lipid vesicles is appreciably higher than that of planar membranes.[24,39]

Within this context, it deserves attention that, using neutron spin−echo (NSE) spectroscopy, Chakraborty et al. found that the magnitude of the bending rigidity of DOPC lipid vesicles (<100 nm) is strongly affected by the cholesterol fraction in the vesicles, demonstrating a roughly 3-fold increase in bending rigidity as the cholesterol content in the vesicle was increased up to ∼50 mol %.[17] In our study, we also observed that cholesterol incorporation appeared to increase the membrane bending energy of sub-100 nm lipid vesicles, while the effect of varying the specific cholesterol fraction was relatively weak in terms of affecting the extent of multivalency-induced vesicle shape deformation. We have, however, explained that this weak effect can be rationalized by an appreciable cholesterol-mediated increase in the lipid bilayer bending rigidity. Thus, our conclusions are in line with those by Chakraborty et al.[17]

In this context, we can add that in our case the scale of the ligand−receptor interaction energy is known, and by analyzing the scale of vesicle deformation, we can in principle estimate the scale of the bending rigidity for the lipid vesicles we use. In the absence of cholesterol, it was done earlier.[27,28] With cholesterol, the rigidity is higher, but its scale is the same. For this reason, we do not perform additional estimates along this line.

In our discussion of the effect of cholesterol on the shape of attached vesicles, we referred above to the multivalent ligand−receptor interaction and membrane rigidity. As noticed in the Introduction, this subject includes many other more specific interesting aspects. We may add a few related remarks as follows: (i) In principle, cholesterol can induce the formation of cholesterol-rich domains in a vesicle. This effect is, however, usually observed in lipid bilayers containing lipids of at least two types. To our knowledge, domains have not been observed in bilayers containing only DOPC lipids, and we believe that

https://doi.org/10.1021/acs.langmuir.2c02252
Langmuir XXXX, XXX, XXX−XXX

the domain formation is not relevant to our case. (ii) Cholesterol molecules can in principle associate with biotinylated lipid molecules as in the case of transmembrane proteins briefly described in the Introduction, and there is some evidence that the presence of cholesterol can reduce the binding availability of lipid headgroups.[42,43] Cholesterol molecules are, however, located inside the lipid bilayer where the structure of biotinylated lipids is the same as that of ordinary lipids while biotin moieties are located outside lipid headgroups. For this reason, the sensitivity of cholesterol to the biotinylated lipid fraction is expected to be weak, and this factor appears to not be relevant as well. (iii) Cholesterol molecules can undergo flip-flop and relax local stresses induced by bending deformations. Although, in principle, this effect can be relevant quantitatively in our case, it does not affect the qualitative interpretation of the results.

CONCLUSION

In this study, we have investigated how cholesterol incorporation into sub-100 nm lipid vesicles affects multivalency-induced shape deformation of the vesicles when binding to a receptor-functionalized SLB platform. While cholesterol is generally known to cause membrane stiffening and higher cholesterol fractions can induce a series of membrane phase transformations depending on the exact lipid compositions, our findings reveal a broader effect of cholesterol to suppress multivalency-induced shape deformation of attached vesicles across the tested range of cholesterol fractions. The LSPR technique enabled these findings by sensitively detecting subtle changes within the vesicle-SLB contact region in terms of vesicle contact radius, height, and fractional surface area contact, depending on the cholesterol fraction in the vesicles and the degree of multivalent binding interactions in the system. The wide range of cholesterol fractions that could suppress multivalency-induced vesicle shape deformation demonstrates that even a relatively small degree of membrane reinforcement enabled by cholesterol incorporation in the high membrane curvature regime can have a significant effect on important structural transformations that are relevant to understanding key biological and biotechnology processes such as membrane-enveloped virus particle infectivity and lipid nanoparticle internalization by cells. While the biophysical insights obtained in this study pertain to lamellar-phase lipid vesicles, such effects of cholesterol might be further explored across a wider range of LNPs (e.g., cubosomes, lipoplexes).[44−46]

ASSOCIATED CONTENT

Supporting Information

The Supporting Information is available free of charge at https://pubs.acs.org/doi/10.1021/acs.langmuir.2c02252.

Vesicle deformation analysis from LSPR data, vesicle compositions (Table S1), summary of parameters used for analytical calculations (Table S2), summary of attached vesicle surface concentrations (Table S3), and additional LSPR data (Figures S1−S3) (PDF)

AUTHOR INFORMATION

Corresponding Authors

Joshua A. Jackman − *School of Chemical Engineering and Translational Nanobioscience Research Center, Sungkyunkwan University, Suwon 16419, Republic of Korea;* orcid.org/0000-0002-1800-8102; Email: jjackman@skku.edu

Nam-Joon Cho − *School of Materials Science and Engineering, Nanyang Technological University, Singapore 637553, Singapore;* orcid.org/0000-0002-8692-8955; Email: njcho@ntu.edu.sg

Authors

Hyeonjin Park − *School of Chemical Engineering and Translational Nanobioscience Research Center, Sungkyunkwan University, Suwon 16419, Republic of Korea; School of Materials Science and Engineering, Nanyang Technological University, Singapore 637553, Singapore*

Tun Naw Sut − *School of Chemical Engineering and Translational Nanobioscience Research Center, Sungkyunkwan University, Suwon 16419, Republic of Korea*

Bo Kyeong Yoon − *School of Healthcare and Biomedical Engineering, Chonnam National University, Yeosu 59626, Republic of Korea*

Vladimir P. Zhdanov − *Division of Nano and Biophysics, Department of Physics, Chalmers University of Technology, Gothenburg 41296, Sweden; Boreskov Institute of Catalysis, Russian Academy of Sciences, Novosibirsk 630090, Russia;* orcid.org/0000-0002-0167-8783

Complete contact information is available at: https://pubs.acs.org/10.1021/acs.langmuir.2c02252

Notes

The authors declare no competing financial interest.

ACKNOWLEDGMENTS

This work was supported by the National Research Foundation of Korea (NRF) grants funded by the Korean government (MSIT; Nos. 2020R1C1C1004385 and 2021R1A4A1032782), the International Research & Development Program of the National Research Foundation of Korea (NRF) funded by the Ministry of Science and ICT (2020K1A3A1A39112724), and a grant of the Korea Health Technology R&D Project through the Korea Health Industry Development Institute (KHIDI), funded by the Ministry of Health & Welfare, Republic of Korea (Grant Number: HI19C1328). This work was also partially supported by the SKKU Global Research Platform Research Fund, Sungkyunkwan University, 2022. Schematic illustrations were created with BioRender.com under an academic lab subscription.

REFERENCES

(1) Pick, H.; Alves, A. C.; Vogel, H. Single-Vesicle Assays Using Liposomes and Cell-Derived Vesicles: From Modeling Complex Membrane Processes to Synthetic Biology and Biomedical Applications. *Chem. Rev.* **2018**, *118* (18), 8598−8654.

(2) Enkavi, G.; Javanainen, M.; Kulig, W.; Róg, T.; Vattulainen, I. Multiscale Simulations of Biological Membranes: The Challenge to Understand Biological Phenomena in a Living Substance. *Chem. Rev.* **2019**, *119* (9), 5607−5774.

(3) Chng, C.-P.; Hsia, K. J.; Huang, C. Modulation of Lipid Vesicle−Membrane Interactions by Cholesterol. *Soft Matter* **2022**, *18*, 7752.

(4) Hajj, K. A.; Whitehead, K. A. Tools for Translation: Non-Viral Materials for Therapeutic mRNA Delivery. *Nat. Rev. Mater.* **2017**, *2* (10), 1−17.

(5) Hou, X.; Zaks, T.; Langer, R.; Dong, Y. Lipid Nanoparticles for mRNA Delivery. *Nat. Rev. Mater.* **2021**, *6* (12), 1078−1094.

(6) Eid, J.; Razmazma, H.; Jraij, A.; Ebrahimi, A.; Monticelli, L. On Calculating the Bending Modulus of Lipid Bilayer Membranes from Buckling Simulations. *J. Phys. Chem. B* **2020**, *124* (29), 6299−6311.
(7) Karal, M. A. S.; Mokta, N. A.; Levadny, V.; Belaya, M.; Ahmed, M.; Ahamed, M. K.; Ahammed, S. Effects of Cholesterol on the Size Distribution and Bending Modulus of Lipid Vesicles. *PLoS One* **2022**, *17* (1), e0263119.
(8) Sut, T. N.; Park, S.; Choe, Y.; Cho, N.-J. Characterizing the Supported Lipid Membrane Formation from Cholesterol-Rich Bicelles. *Langmuir* **2019**, *35* (47), 15063−15070.
(9) van der Koog, L.; Gandek, T. B.; Nagelkerke, A. Liposomes and Extracellular Vesicles as Drug Delivery Systems: A Comparison of Composition, Pharmacokinetics, and Functionalization. *Adv. Healthcare Mater.* **2022**, *11* (5), 2100639.
(10) Sorre, B.; Callan-Jones, A.; Manneville, J.-B.; Nassoy, P.; Joanny, J.-F.; Prost, J.; Goud, B.; Bassereau, P. Curvature-Driven Lipid Sorting Needs Proximity to a Demixing Point and is Aided by Proteins. *Proc. Natl. Acad. Sci. U. S. A.* **2009**, *106* (14), 5622−5626.
(11) Pan, J.; Tristram-Nagle, S.; Nagle, J. F. Effect of Cholesterol on Structural and Mechanical Properties of Membranes Depends on Lipid Chain Saturation. *Phys. Rev. E* **2009**, *80* (2), 021931.
(12) Rawicz, W.; Smith, B.; McIntosh, T.; Simon, S.; Evans, E. Elasticity, Strength, and Water Permeability of Bilayers That Contain Raft Microdomain-Forming Lipids. *Biophys. J.* **2008**, *94* (12), 4725−4736.
(13) Pan, J.; Mills, T. T.; Tristram-Nagle, S.; Nagle, J. F. Cholesterol Perturbs Lipid Bilayers Nonuniversally. *Phys. Rev. Lett.* **2008**, *100* (19), 198103.
(14) Henriksen, J.; Rowat, A. C.; Brief, E.; Hsueh, Y.; Thewalt, J.; Zuckermann, M.; Ipsen, J. H. Universal Behavior of Membranes with Sterols. *Biophys. J.* **2006**, *90* (5), 1639−1649.
(15) Henriksen, J.; Rowat, A. C.; Ipsen, J. H. Vesicle Fluctuation Analysis of the Effects of Sterols on Membrane Bending Rigidity. *Eur. Biophys. J.* **2004**, *33* (8), 732−741.
(16) Meleard, P.; Gerbeaud, C.; Pott, T.; Fernandez-Puente, L.; Bivas, I.; Mitov, M. D.; Dufourcq, J.; Bothorel, P. Bending Elasticities of Model Membranes: Influences of Temperature and Sterol Content. *Biophys. J.* **1997**, *72* (6), 2616−2629.
(17) Chakraborty, S.; Doktorova, M.; Molugu, T. R.; Heberle, F. A.; Scott, H. L.; Dzikovski, B.; Nagao, M.; Stingaciu, L.-R.; Standaert, R. F.; Barrera, F. N.; et al. How Cholesterol Stiffens Unsaturated Lipid Membranes. *Proc. Natl. Acad. Sci. U. S. A.* **2020**, *117* (36), 21896−21905.
(18) Gracià, R. S.; Bezlyepkina, N.; Knorr, R. L.; Lipowsky, R.; Dimova, R. Effect of Cholesterol on the Rigidity of Saturated and Unsaturated Membranes: Fluctuation and Electrodeformation Analysis of Giant Vesicles. *Soft Matter* **2010**, *6* (7), 1472−1482.
(19) Nagle, J. F. Measuring the Bending Modulus of Lipid Bilayers with Cholesterol. *Phys. Rev. E* **2021**, *104* (4), 044405.
(20) Mathai, J. C.; Tristram-Nagle, S.; Nagle, J. F.; Zeidel, M. L. Structural Determinants of Water Permeability through the Lipid Membrane. *J. Gen. Physiol.* **2008**, *131* (1), 69−76.
(21) Lipowsky, R. Coupling of Bending and Stretching Deformations in Vesicle Membranes. *Adv. Colloid Interface Sci.* **2014**, *208*, 14−24.
(22) Kulkarni, J. A.; Myhre, J. L.; Chen, S.; Tam, Y. Y. C.; Danescu, A.; Richman, J. M.; Cullis, P. R. Design of Lipid Nanoparticles for in Vitro and in Vivo Delivery of Plasmid DNA. *Nanomed.: Nanotechnol. Biol. Med.* **2017**, *13* (4), 1377−1387.
(23) Ermilova, I.; Swenson, J. DOPC Versus DOPE as a Helper Lipid for Gene-Therapies: Molecular Dynamics Simulations with DLin-MC3-DMA. *Phys. Chem. Chem. Phys.* **2020**, *22* (48), 28256−28268.
(24) Takechi-Haraya, Y.; Sakai-Kato, K.; Abe, Y.; Kawanishi, T.; Okuda, H.; Goda, Y. Atomic Force Microscopic Analysis of the Effect of Lipid Composition on Liposome Membrane Rigidity. *Langmuir* **2016**, *32* (24), 6074−6082.
(25) Vorselen, D.; MacKintosh, F. C.; Roos, W. H.; Wuite, G. J. Competition between Bending and Internal Pressure Governs the Mechanics of Fluid Nanovesicles. *ACS Nano* **2017**, *11* (3), 2628−2636.
(26) Sorkin, R.; Huisjes, R.; Bošković, F.; Vorselen, D.; Pignatelli, S.; Ofir-Birin, Y.; Freitas Leal, J. K.; Schiller, J.; Mullick, D.; Roos, W. H.; et al. Nanomechanics of Extracellular Vesicles Reveals Vesiculation Pathways. *Small* **2018**, *14* (39), 1801650.
(27) Park, H.; Sut, T. N.; Yoon, B. K.; Zhdanov, V. P.; Cho, N.-J.; Jackman, J. A. Unraveling How Multivalency Triggers Shape Deformation of Sub-100 nm Lipid Vesicles. *J. Phys. Chem. Lett.* **2021**, *12* (28), 6722−6729.
(28) Park, H.; Sut, T. N.; Yoon, B. K.; Zhdanov, V. P.; Kim, J. W.; Cho, N.-J.; Jackman, J. A. Multivalency-Induced Shape Deformation of Nanoscale Lipid Vesicles: Size-Dependent Membrane Bending Effects. *J. Phys. Chem. Lett.* **2022**, *13*, 1480−1488.
(29) Norling, K.; Sjöberg, M.; Bally, M.; Zhdanov, V. P.; Parveen, N.; Höök, F. Dissimilar Deformation of Fluid-and Gel-Phase Liposomes Upon Multivalent Interaction with Cell Membrane Mimics Revealed Using Dual-Wavelength Surface Plasmon Resonance. *Langmuir* **2022**, *38*, 2550.
(30) Jackman, J. A.; Cho, N.-J. Supported Lipid Bilayer Formation: Beyond Vesicle Fusion. *Langmuir* **2020**, *36* (6), 1387−1400.
(31) MacDonald, R. C.; MacDonald, R. I.; Menco, B. P. M.; Takeshita, K.; Subbarao, N. K.; Hu, L.-r. Small-Volume Extrusion Apparatus for Preparation of Large, Unilamellar Vesicles. *Biochim. Biophys. Acta, Biomembr.* **1991**, *1061* (2), 297−303.
(32) Jackman, J. A.; Zhdanov, V. P.; Cho, N.-J. Nanoplasmonic Biosensing for Soft Matter Adsorption: Kinetics of Lipid Vesicle Attachment and Shape Deformation. *Langmuir* **2014**, *30* (31), 9494−9503.
(33) Langhammer, C.; Larsson, E. M.; Kasemo, B.; Zoric, I. Indirect Nanoplasmonic Sensing: Ultrasensitive Experimental Platform for Nanomaterials Science and Optical Nanocalorimetry. *Nano Lett.* **2010**, *10* (9), 3529−3538.
(34) Fredriksson, H.; Alaverdyan, Y.; Dmitriev, A.; Langhammer, C.; Sutherland, D. S.; Zäch, M.; Kasemo, B. Hole−Mask Colloidal Lithography. *Adv. Mater.* **2007**, *19* (23), 4297−4302.
(35) Kennedy, G.; Buiu, O.; Taylor, S. Oxidation of Silicon Nitride Films in an Oxygen Plasma. *J. Appl. Phys.* **1999**, *85* (6), 3319−3326.
(36) Dahlin, A. B.; Tegenfeldt, J. O.; Höök, F. Improving the Instrumental Resolution of Sensors Based on Localized Surface Plasmon Resonance. *Anal. Chem.* **2006**, *78* (13), 4416−4423.
(37) Hinrichsen, E. L.; Feder, J.; Jøssang, T. Geometry of Random Sequential Adsorption. *J. Stat. Phys.* **1986**, *44* (5), 793−827.
(38) Jackman, J. A.; Špačková, B.; Linardy, E.; Kim, M. C.; Yoon, B. K.; Homola, J.; Cho, N.-J. Nanoplasmonic Ruler to Measure Lipid Vesicle Deformation. *Chem. Commun.* **2016**, *52* (1), 76−79.
(39) Jackman, J. A.; Yorulmaz Avsar, S.; Ferhan, A. R.; Li, D.; Park, J. H.; Zhdanov, V. P.; Cho, N.-J. Quantitative Profiling of Nanoscale Liposome Deformation by a Localized Surface Plasmon Resonance Sensor. *Anal. Chem.* **2017**, *89* (2), 1102−1109.
(40) Jin, Y.; Chen, J.; Xu, L.; Wang, P. Refractive Index Measurement for Biomaterial Samples by Total Internal Reflection. *Phys. Med. Biol.* **2006**, *51* (20), N371.
(41) Ashkar, R.; Doktorova, M.; Heberle, F. A.; Scott, H. L.; Barrera, F. N.; Katsaras, J.; Khelashvili, G.; Brown, M. F. Reply to Nagle Et Al.: The Universal Stiffening Effects of Cholesterol on Lipid Membranes. *Proc. Natl. Acad. Sci. U. S. A.* **2021**, *118* (20), e2102845118.
(42) Lingwood, D.; Binnington, B.; Róg, T.; Vattulainen, I.; Grzybek, M.; Coskun, Ü.; Lingwood, C. A.; Simons, K. Cholesterol Modulates Glycolipid Conformation and Receptor Activity. *Nat. Chem. Biol.* **2011**, *7* (5), 260−262.
(43) Mahfoud, R.; Manis, A.; Binnington, B.; Ackerley, C.; Lingwood, C. A. A Major Fraction of Glycosphingolipids in Model and Cellular Cholesterol-Containing Membranes is Undetectable by Their Binding Proteins. *J. Biol. Chem.* **2010**, *285* (46), 36049−36059.
(44) Rubio, L.; Alonso, C.; Rodríguez, G.; Cócera, M.; López-Iglesias, C.; Coderch, L.; De la Maza, A.; Parra, J.; López, O. Bicellar Systems as New Delivery Strategy for Topical Application of Flufenamic Acid. *Int. J. Pharm.* **2013**, *444* (1−2), 60−69.

https://doi.org/10.1021/acs.langmuir.2c02252
Langmuir XXXX, XXX, XXX−XXX

(45) Kranz, L. M.; Diken, M.; Haas, H.; Kreiter, S.; Loquai, C.; Reuter, K. C.; Meng, M.; Fritz, D.; Vascotto, F.; Hefesha, H.; et al. Systemic RNA Delivery to Dendritic Cells Exploits Antiviral Defence for Cancer Immunotherapy. *Nature* **2016**, *534* (7607), 396−401.
(46) Bost, J. P.; Barriga, H.; Holme, M. N.; Gallud, A.; Maugeri, M.; Gupta, D.; Lehto, T.; Valadi, H.; Esbjörner, E. K.; Stevens, M. M.; El-Andaloussi, S. Delivery of Oligonucleotide Therapeutics: Chemical Modifications, Lipid Nanoparticles, and Extracellular Vesicles. *ACS Nano* **2021**, *15* (9), 13993−14021.

https://doi.org/10.1021/acs.langmuir.2c02252
Langmuir XXXX, XXX, XXX−XXX